On the evolution of chaperones and co-chaperones and the exponential expansion of proteome complexity

Authors: Mathieu E. Rebeaud[1]*, Saurav Mallik[2]*, Pierre Goloubinoff[1]† and Dan S. Tawfik[2]†

Author affiliations:

[1] Department of Plant Molecular Biology, Faculty of Biology and Medicine, University of Lausanne, CH-1015 Lausanne, Switzerland.

[2] Department of Biomolecular Sciences, The Weizmann Institute of Science, Rehovot 7610001, Israel.

* Equally contributing first authors

† Correspondence: Pierre.Goloubinoff@unil.ch; dan.tawfik@weizmann.ac.il

Lead Contact: D.S.T. (dan.tawfik@weizmann.ac.il)

Summary

Along evolutionary time, starting from simple a beginning, the repertoire of life's proteins has widely expanded. A systematic analysis across the Tree of Life (ToL) depicts that from simplest archaea to mammals, the total number of proteins per proteome expanded ~200-fold. In parallel, proteins became more complex: protein length increased ~3-fold, and multi-domain proteins expanded ~300-fold. Apart from duplication and divergence of existing proteins, expansion was driven by birth of completely new proteins. Along the ToL, the number of different folds expanded ~10-fold, and fold-combinations ~40-fold. Proteins prone to misfolding and aggregation, such as repeat and beta-rich proteins, proliferated ~600-fold. To control the quality of these exponentially expanding proteomes, core-chaperones, ranging from HSP20s that prevent aggregation, to HSP60, HSP70, HSP90 and HSP100 acting as ATP-fueled unfolding and refolding machines, also evolved. However, these core-chaperones were already available in prokaryotes ~3 billion years ago, and expanded linearly, as they comprise ~0.3% of all genes from archaea to mammals. This challenge—roughly the same number of core-chaperones supporting an exponential expansion of proteome complexity, was met by: (i) higher cellular abundances of the ancient generalist core-chaperones, and (ii) continuous emergence of new substrate-binding and nucleotide-exchange factor co-chaperones that function cooperatively with core-chaperones, as a network.

Keywords

Tree of Life, expansion of proteomes, proteome complexity, core-chaperones, co-chaperones, chaperone network

Introduction

All cellular life is thought to have stemmed from the Last Universal Common Ancestor, LUCA (Doolittle, 1999; Woese, 1998), that emerged more than 3.6 billion years ago. Two major kingdoms of life diverged from LUCA: bacteria and archaea, which about 2 billion years later merged into the eukaryotes (Eme et al., 2017). Since the beginning of biological evolution, life's volume has increased on a grand scale: the average size of individual cells has increased ~100-fold from prokaryotes to eukaryotes (Cooper and Hausman, 2000), the number of cell types has increased ~200-fold from unicellular eukaryotes to humans (Arendt, 2008), and average body size increased ~5000 fold from simplest sponges to blue whales (Heim et al., 2017). Life's habitability has also expanded from its specific niche of emergence—likely deep-sea hydrothermal vents, to highly variable and extreme ranges of temperature, pressure, exposure to high UV-light, dehydration and free oxygen.

This expansion in organismal complexity and variability was accompanied by an expansion in life's molecular workforce, proteomes in particular, which in turn presented a challenge of reaching and maintaining properly folded and functional proteomes. Most proteins must fold to their native structure in order to function, and their folding is largely imprinted in their primary amino acid sequence (Anfinsen, 1973; Dill and Chan, 1997; Englander and Mayne, 2014). However, many proteins, and especially large multi-domain polypeptides, or certain protein types such as all-beta or repeat proteins, tend to misfold and aggregate into inactive species that may also be toxic (Han et al., 2007). Life met this challenge by evolving molecular chaperones that can minimize protein misfolding and aggregation, even under stressful out-of-equilibrium conditions favoring aggregation (Finka et al., 2016; Kim et al., 2013). Alongside the core-chaperones HSP20, HSP60, HSP70, HSP100 and HSP90, that are mostly ATPases, a variety of co-chaperones has emerged that facilitate and modulate the basal protein holding, unfolding and refolding activities of the core-chaperones (Caplan, 2003; Duncan et al., 2015; Schopf et al., 2017).

Starting from LUCA, as proteome complexity expanded, so did the core-chaperones and their respective co-chaperones. Indeed, chaperones have been shown to facilitate the acquisition of destabilizing mutations and thereby accelerate protein evolution (Alvarez-Ponce et al., 2019; Bogumil and Dagan, 2012; Tokuriki and Tawfik, 2009). However, the co-expansion of proteomes and of chaperone complexity, underscoring a critical balance between evolutionary innovation and foldability, remains largely unexplored. We thus embarked on a systematic bioinformatic analysis that explores the evolution of both proteome and chaperone complexity, and of both core- and their auxiliary co-chaperones, along the tree of life.

Results

A Tree of Life analysis of the expansion of proteome complexity and chaperones

We aimed to explore the evolutionary history of chaperones, systematically, across the Tree of Life (ToL), alongside the increase in proteome complexity. To this end, we collected proteome sequences from representative organisms belonging to all the major bacterial, archaeal and eukaryotic clades and constructed a ToL (**Figure 1A**) that captures all major divergence events (see **Methods**). We reconciled the topology of our tree with that of the TimeTree (Hedges et al., 2015) that begins ~4100 million years ago (MYA) and adhered to its dating. Some of the dates are putative and may be controversial (*e.g.* LUCA datings span from 3600 to 4100 MYA). Nonetheless, these timelines provide a *relative* time axis against which changes in proteome complexity and chaperone content could be plotted.

The Tree of Life begins with the emergence of the Last Universal Common Ancestor (LUCA) at the root (**Figure 1A**). The edges of the ToL represent the extant clades, and each extant clade comprises at least one representative species (**Data S1**). The nodes represent the hypothetical ancestors. The first node represents the split of the Last Bacterial and Archaeal Ancestors (LBA and LAA, respectively). The emergence of the Last Eukaryotic Common Ancestor (LECA), approximately 2100 MYA, follows the primary endosymbiosis of an *Alphaproteobacterium* into an Asgard-like archaea (de Duve, 2007; Margulis et al., 2006) Roughly 1200 MYA, the emergence of green algae and subsequently of plants occurred with a secondary endosymbiosis of a *Cyanobacterium* into a non-photosynthetic eukaryote (Martin et al., 1998). These two major endosymbiotic events are represented as vertical arrows. The bacterial, archaeal and various eukaryotic clades are highlighted in specific colors that represent them in all subsequent analyses.

Overall, our analysis was based on a core-tree that included the proteomes of 188 representative organisms, covering 56 major clades of bacteria, archaea and eukaryote (**Data S1**). The various proteome parameters analyzed below were initially derived for each representative organism in the core-tree. The representative organisms of each clade were then pulled together to calculate the clade average and the standard deviation for this average. The clade average values were subsequently plotted against their predicted time of divergence.

The expansion of proteome size

Initially, we scrutinized the expansion of proteome size by examining (i) the total number of proteins per proteome in a given clade; (ii) the median protein length; and (iii) the number of multi-domain proteins in the proteome. The clade average values of these three parameters were plotted in **Figure 1B–D**, with colors of points matching with the branch-colors in **Figure 1A**).

The total number of proteins per proteome expanded ~200-fold **(Figure 1B)**. Proteomes that comprise a larger number of proteins unavoidably present a greater challenge for their protein quality control chaperone machinery. Along the ToL, the number of proteins per proteome expanded roughly 200-fold from 536 proteins in the simplest obligate symbiont archaea *Nanoarchaeum equitans*, the closest known derivative of LUCA (Di Giulio, 2007; Waters et al., 2003), to ~120,000 proteins in human (**Data S2**). Within archaea, a 10-fold expansion of proteome size was observed. The largest archaeal proteome of 5,514 proteins belongs to *Candidatus Heimdallarchaeota archaeon* LC_3, which is a member of the Asgard group from which eukaryotes have stemmed out (Fournier and Poole, 2018; MacLeod et al., 2019; Spang et al., 2018). A somewhat smaller 6-fold proteome expansion was observed in bacteria, from 1,508 proteins in the autotrophic sulfur-reducing thermophilic bacterium *Desulfurobacterium thermolithotrophum*, belonging to the earliest diverging bacterial clade *Aquificae* (closest derivative of LBA (Battistuzzi et al., 2004) , to 8,073 proteins in the soil bacteria *Sorangium cellulosum*. A ~20-fold expansion in the number of proteins per proteome was observed in eukaryotes, starting from 6,502 proteins in *Giardia intestinalis*, a parasite considered to be one of the earliest diverging eukaryotes to hundreds of thousands in land plants and chordates, in which most of protein number expansion occurred, apparently due to multiple rounds of large-scale gene and whole genome duplications that accompanied their emergence (Van de Peer et al., 2009). However, as described later, this dramatic increase in the number of proteins occurred not only by duplication of pre-existing proteins, but also by emergence of completely new domains and folds.

The median protein length increased ~3-fold **(Figure 1C)**. The longer the polypeptides are, with larger domains and/or multiple domains, the more prone they are to misfold and aggregate, instead of readily reaching their native functional state (Henzler-Wildman and Kern, 2007; Mayer, 2010). Along the ToL, median protein length increased about 3-fold, starting from ~200 residues in *Nanoarchaea* to ~500 residues in chordata (**Data S2**). Longer proteins were found primarily in multicellular eukaryotes (average lengths of the top 10% largest proteins were roughly 1,300 residues in plants, ~1,500 residues in metazoan, and ~2,150 residues in mammals). The longest polypeptides in mammals are predominantly muscle proteins, including different variants of titin (> 34,000 residues) or adhesins (> 5000 residues).

There are different ways by which proteins can increase in size. Firstly, the domains themselves can grow larger by decorating an ancestral core domain with additional segments. Secondly, fusion of multiple domains can result in a larger multi-domain protein. Thirdly, domain-flanking regions (C- and N-termini segments, and inter-domain linkers), that are typically disordered, can expand. A systematic analysis of 38 distinct folds that could be traced back to LUCA showed that lengths of individual domains increased mildly, nearly 1.5-fold, across the ToL (**Figure S1A, Data S2**). The expansion of domain-flanking segments was also modest, nearly 3-fold, from simplest archaea to multicellular

eukaryotes (**Figure S1B, Data S2**). Indeed, as elaborated below, length expansion primarily stemmed from the increase in the fraction of multi-domain proteins.

Multi-domain proteins expanded ~300-fold **(Figure 1D)**. Multi-domain proteins are inherently more prone to misfolding and aggregation than single domain proteins, and may therefore demand more chaperone holding-unfolding-refolding action (Gong et al., 2009; Lafita et al., 2019; Liu et al., 2019). Along the ToL, multi-domain proteins comprising ≥ 3 Pfam-annotated domains have expanded ~300-fold, from only 21 in *Nanoarchaeota* to 6962 in *Zea mays* (**Data S2**). Multi-domain proteins have in fact expanded beyond the expansion of proteome size, to become nearly 3-fold more frequent (**Figure S1C**) with the expected corresponding shrinkage of proteins comprising 1–2 domains, **Figure S1D**). As described later, this expansion occurred not only by duplication of pre-existing multi-domain proteins, but foremost by the emergence of new domain combinations.

The expansion of proteome complexity

Most proteins emerge by duplication and divergence of a pre-existing protein. Thus, for paralogous proteins with the same overall fold and domain arrangement (for multi-domain proteins), expansion can be considered as 'linear'. In other words, duplication and 'local' divergence (point mutations and short insertions or deletions) certainly increase proteome size (total number of proteins) but not proteome complexity. The latter relates primarily to the birth of completely new proteins possessing new folds, and to the emergence of multi-domain proteins with new fold combinations. Proteome expansion by birth of new folds and fold-combinations would be considered 'exponential', because proteome composition significantly changes and expands beyond proteome size. We thus reanalyzed additional proteome parameters that represent exponential, rather than linear expansion, as detailed below.

Fold-types expanded ~10-fold **(Fig 2A**). Compared to emergence by duplication of a pre-exiting protein, the birth of a completely new protein is an unforeseen task that must impose a larger burden on chaperones. To assess the emergence of new folds, we used ECOD—a hierarchical classification of protein folds that uses both sequence and structural similarities and clusters all domains with known structures into independently evolved lineages, termed as the 'X-groups' (Schaeffer et al., 2016). We found that along the ToL, the number of unique folds expanded about 10-fold, from only 38 unique X-groups in *Nanoarchaeota* to 474 in human (**Data S3**).

New fold-combinations expanded ~40-fold **(Fig 4B)**. We showed above that multi-domain proteins expanded nearly 3-fold (their fraction out to the total number of proteins), alongside a parallel shrinkage of proteins comprising 1–2 domains (**Fig S1 C, D**). This expansion of multi-domain proteins was not merely by duplication, namely by amplifying pre-existing multi-domain proteins, but also owing to the emergence of new combinations. To assess the latter, we examined the number of unique vectorial combinations of domains per proteome, with domains being assigned by ECOD X-groups. It appeared

that new domain combinations arose throughout evolution, with an overall increase of ~40-fold, from 58 combinations in *Nanoarchaeota* to 2430 combinations in human (**Data S4, S5**).

All-beta and beta-rich folds expanded up to ~600-fold **(Fig 4C**). Proteins that are beta-rich are known to be prone to misfolding and aggregation (Pawar et al., 2005). In the simplest bacteria and archaea, proteins comprising the ancient all-alpha and alpha-beta architectures are the most frequent. Remarkably, upon the emergence of eukaryotes, and in metazoans especially, all-beta or beta-rich architectures (beta-superfold) expanded massively (**Fig S2**) and became nearly 6-fold more frequent in mammalian proteomes, as compared to *Nanoarchaeota* (*i.e.*, in proportion to the total number of proteins, **Data S6**). The immunoglobulin fold had a major contribution to this expansion, owing to its diverse roles in immunity, multi-cellularity and signaling (Halaby and Mornon, 1998).

Repeat sequences expanded ~700-fold (**Fig 4D**). Proteins comprising tandem repeats of nearly identical sequences emerge readily yet are prone to misfolding and aggregation. We identified proteins with repeated sequences of the size of a single 'foldon' unit, ~20 aa (Englander and Mayne, 2014), with ≥ 90% sequence similarity (**Data S7**). No such repeated sequences were detected in the earliest diverging archaea and bacteria (*Nanoarchaeota* and DPANN group, and *Thermotogae*). However, these repeats began to appear in more recently diverged prokaryotes and expanded massively in eukaryotes (a similar trend was described in (Andrade et al., 2001)). Indeed, metazoan proteomes contain large proteins with long repeated segments, *e.g. Drosophila* Ank2p (21 Ankyrin repeats, in total 836 residues), or human Dmbt1p (11 cysteine-rich repeats of total 1419 residue length). The cumulative length of repeat sequences in metazoan proteomes can be up to 100,000 residues. Overall, a 700-fold expansion of repeated sequences was observed along the ToL (**Figure S3, Data S2**). Repeated sequences also expanded beyond the expansion of proteome size – the percent of total proteome length that comprises repeats increased nearly 7-fold from the simplest archaea to metazoans (sum of repeat lengths normalized by the sum of all protein lengths; **Figure 4D**).

Overall, it appears that although gene and whole-genome duplications dominate, and in particular along the evolution of eukaryotes (Van de Peer et al., 2009), dramatic expansion in proteome complexity has occurred owing to *bona fide* innovations. Specifically, in relation to the burden on the chaperone machinery, proteomes have expanded exponentially with respect to new folds, beta-superfolds, repeat proteins, and fold combinations.

The evolutionary history of chaperones

In parallel to estimating the expansion of proteome complexity, we investigated the evolutionary history of chaperones, aiming to date their emergence and their expansion along the ToL. To that end, absence or presence, and copy numbers, of the core-chaperones (HSP20, HSP60, HSP70, HSP100, and HSP90) was determined for the representative proteomes. Subsequently, protein trees were generated and

compared with the ToL, to account for gene loss and horizontal transfer events. Protein sequences of all core-chaperones families were extracted from the representative proteomes (**Data S8**). These sequences were aligned and were used to generate maximum likelihood, midpoint-rooted protein trees which were then compared with the ToL (see **Methods**, **Table S1**).

The core-chaperones emerged in early-diverging prokaryotes (**Fig 3A**). Our analysis traced the origin of all five core-chaperone families in early-diverging prokaryotes. Two universally distributed chaperone families, HSP20—an anti-aggregation 'holding' chaperone, and HSP60—a cage-like ATP-fueled unfoldase (Finka et al., 2016; Saibil, 2013) were assigned to LUCA, consistent with previous work (Sousa et al., 2016; Weiss et al., 2016). The protein tree of HSP20, the only ATP-independent core chaperone, depicts a bacteria-archaea split at its root, albeit with rather weak bootstrap support and multiple indications of horizontal transfers between bacteria and archaea (**Fig 3B**, **Table S1**; as noted before (Kriehuber et al., 2010)). The HSP60 protein tree also depicts a bacteria-archaea split, and with a strong bootstrap support (**Table S1**). It therefore seems that HSP60 has rarely been horizontally transferred between bacteria and archaea, with two notable exceptions, an ancient transfer from archaea to Firmicutes (Techtmann and Robb, 2010) and the other from *Spirochaetia* to *Euryarchaeota* (**Fig 3B**).

The remaining core-chaperone families, HSP70, HSP90 and HSP100 appear to have emerged in bacteria, ~1 billion years after LUCA, though extensive horizontal transfer between different bacterial clades, and between bacteria and archaea, prevent the reliable assignment of their points of origin (**Fig 3A**, **3B**). The ATP-dependent core-chaperone HSP70—that controls protein unfolding, disaggregation, translocation and degradation (Fernandez-Fernandez and Valpuesta, 2018; Rosenzweig et al., 2019), was detected in the earliest diverging bacterial clades *Aquificae* and *Thermotogae*. However, the protein tree indicated that these phyla borrowed HSP70 from the later-diverging bacterial lineages, such as *Deltaproteobacteria*, *Clostridia* and *Bacilli* (**Fig 3B**, **Table S1**). HSP70 appears to have a bacterial origin, around or after the emergence of terrestrial bacteria (*i.e.*, around the divergence of *Fusobacteria* (Battistuzzi and Hedges, 2009)), *ca.* 1 billion years after HSP20 and HSP60 have emerged (**Fig 3A**). Following its emergence, HSP70 has been extensively horizontally transferred to major archaeal clades including TACK group, *Euryarchaeota* and Asgard group (**Figure 3B**).

The protein trees of both HSP90 and HSP100 depict a similar scenario. Both seem to have emerged in bacteria around or after terrestrial bacteria emerged (**Figure 3A**) and have subsequently been horizontally transferred to bacterial clades that diverged earlier, as well as to archaea (**Figure 3B**, **Table S1**). Although a reliable point of origin could not be assigned for either of these two chaperones, biochemical assays show that whereas the activity of HSP90 or HSP100 strictly depends on the presence of HSP70, HSP70 can act independently. Further, across the ToL, every organism that harbors genes for Hsp90 and or HSP100 also harbors genes for HSP70, but not *vice versa*. Thus, it is likely that HSP90 and HSP100 have both emerged after HSP70.

The archaeal and bacterial core chaperones were integrated into LECA, and no new core-chaperones emerged with the birth of eukaryotes (**Figure 3A**). Chaperones of archaeal origin mostly continued to function in their original compartment, the cytosol. Although most *Alphaproteobacterial* endosymbiont genes were transferred to the nucleus, most of the chaperones of bacterial origin evolved to translocate back to the compartment from which they originated, namely to the mitochondria (Bogumil et al., 2014; Hemmingsen et al., 1988; Kampinga et al., 2019; Martin et al., 2002). Chaperone evolution in eukaryotes involved gene loss as well, *e.g.*, cytosolic and mitochondrial HSP100 have been lost in metazoa (Kampinga et al., 2019).

***Core-chaperones expanded linearly* (Fig 3C)**. Whereas no new core-chaperone family emerged in the last ~3 billion years, gene copy numbers of the existing families did increase via gene duplication, to support expanding proteomes, for condition-specific expression and also to cater for the emergence of multiple subcellular compartments. Accordingly, in bacterial and archaeal proteomes, copy numbers of individual core-chaperone families range between 1–4, summing up to an average of ~8 core-chaperones per proteome (**Figure S4**, **Data S8**). Overall, the total number of core-chaperones per proteome expanded about 3-fold in bacteria and about 5-fold in archaea. Core-chaperones expanded more drastically in eukaryotes. Compared to the simplest eukaryotes, the number of chaperones in higher plants, which are among the most complex eukaryotes, increased ~30-fold for HSP20 (**Fig S4A**), ~50-fold for HSP60 (**Fig S4B**), ~40-fold for HSP70 (**Fig S4C**), ~20-fold for HSP90 (**Fig S4D**), and ~10-fold for HSP100 (**Fig S4E**). Parasitic microbes, such as *Mycoplasma pneumoniae*, *Plasmodium falciparum*, and *Entamoeba histolytica*, and photosynthetic bacteria, algae and plants often harbor unusually high chaperone gene copy numbers, likely to counter the immune response of the host (Day et al., 2019; Shonhai et al., 2011) and the oxidative stress (Dahl et al., 2015; Niforou et al., 2014). Notably, the expansion of core-chaperone genes largely coincides with the overall expansion of proteome size. Core-chaperones comprise ~0.3%, *i.e.*, 3 out of 1000 proteins, in all proteomes, from the simplest archaea to mammals (**Figure 3C**). Thus, in contrast to proteome complexity, core-chaperones expanded rather 'linearly': no *bona fide* innovation occurred in the last ~3 billion years, and their gene copy-numbers did not expand beyond proteome size.

***Core-chaperones became ~6-fold more abundant in the cell* (Figure 3D)**. While copy numbers of core-chaperone genes remained roughly constant, perhaps their abundance increased instead to support the expansion of proteome complexity? To examine this, the relative basal abundance of core- or co-chaperones in the cell was compared. Unfortunately, this analysis is restricted to model organisms in which ample proteomics data are available. Non-redundant proteome-scale abundance data was collected for 11 model organisms spanning 9 major clades along the ToL (see **Methods**, **Data S9**). As plotted in **Figure 3D**, the relative basal abundance of core-chaperones in the cell appears to have increased ~6 fold, from ~0.7% in Firmicutes (the earliest diverging clade for which reliable proteomics data are available) to ~4.0% in mammals.

Co-chaperones expanded ~9-fold **(Figure 3E)**. The gene copy numbers of core-chaperones expanded linearly, and their protein abundance also increased in the cells, yet both these trends comprise more of the same, rather than evolutionary innovation. The latter seems to have occurred primarily with respect to their supporting workforce, namely co-chaperones. The number of unique co-chaperone families expanded from only 1 in DPANN archaea (closest relative to *Nanoarchaea*) to ~20 in human. Most co-chaperones are eukaryote-specific (**Data S8**), and therefore have likely emerged relatively recently, and only a few co-chaperones are found in all three domains of life. To date their emergence, protein trees were generated. These suggest that, as expected, these co-chaperones emerged after the core-chaperone they work with. HSP60 is assigned LUCA, while its bacterial co-chaperone HSP10/GroES appears to have emerged in the LBA (**Figure 3A**, **Table S1**). HSP70's co-chaperones, the J-domain proteins (JDPs) and GrpE, and HSP90's co-chaperone Cyp40, appear to have emerged at the same node as their respective core-chaperones. Given the extensive horizontal transfer and the resolution that protein trees allow, a more precise dating could not be performed. It appears that JDP, GrpE and Cyp40, have all emerged after the emergence of terrestrial bacteria (**Figure 3A**), as was HSP70, and both the core- and its co-chaperones were then horizontally transferred between different bacterial clades and also from bacteria to archaea (**Table S1**). Several co-chaperone families emerged in eukaryotes (**Figure 3A**), including HSP110 that duplicated and diverged from HSP70 (Sarkar et al., 2013), and Pih1, Aha1 and Chip that harbor eukaryote-specific folds and hence likely emerged *de novo*. Overall, it is evident that co-chaperones tail core-chaperones, and not vice versa. With the birth of several co-chaperones in eukaryotes, the percentage of genes encoding for co-chaperones in the proteome expanded ~9-fold from simplest archaea to metazoan (**Figure 3E**). Notably, the JDPs, which are co-chaperones of HSP70, are the major contributor to this copy-number expansion (Bogumil and Dagan, 2012).

This implies that evolutionary innovation occurred primarily at the level of co-chaperones that facilitated the basal core-chaperone activity thus expanding the chaperone network to meet the challenges of newly emerging protein folds and increasingly complex proteomes.

Discussion

How did chaperones evolve to support the expansion of proteome complexity? To address this question, we compiled data from multiple sources and analyzed them under one roof, thus allowing a systematic, quantitative comparison. This study thereby provides a resource for examining both chaperone and proteome evolution along the Tree of Life. This resource includes the mapping of all known protein domains, and domain-combinations, on the Tree of Life, and species and protein trees of all known chaperone families.

Comparison of the expansion of proteome complexity versus that of core-chaperones presents a dichotomy—a linear expansion of core-chaperones supported an exponential expansion of proteome

complexity. We propose that this dichotomy was reconciled by two features that comprise the hallmark of chaperones: the generalist nature of core-chaperones, and their ability to act in a cooperative mode alongside co-chaperones as an integrated network. Indeed, in contrast to core-chaperones, there exist a consistent trend of evolutionary expansion of co-chaperones.

HSP60, HSP70, HSP90 and HSP100 are core-chaperones acting as generalist unfolding-refolding machineries that work on a broad range of differently misfolded and aggregated protein substrates, largely regardless of size (except HSP60 (Bukau and Horwich, 1998)), structure and function (Finka et al., 2016; Gong et al., 2009). While core-chaperones can exert high affinity binding to few specific substrates at their native folded state, they generally tend to bind misfolded and aggregated polypeptides that abnormally expose hydrophobic surfaces (Gong et al., 2009; Rudiger et al., 1997; Scheibel et al., 1998). The main driving force for duplication and specialization is a functional tradeoff—optimization of one function comes at the expense of other functions (Tawfik and Gruic-Sovulj, 2020). However, given a 'generalist' mode of function, the quality-control of increasingly complex proteomes could be achieved by an increase in abundance of core-chaperones, rather than by the emergence of new core-chaperone families. Although gene copy-numbers of core-chaperones have indeed increased by gene duplication, and the resulting paralogous copies have mostly re-localized to different subcellular compartments or are expressed under different stress conditions (Kampinga et al., 2009). In parasitic microbes and photosynthetic organisms, duplicates of HSP70 and HSP90 have sub-specialized to resist host immune responses and oxidative stress (Dahl et al., 2015; Day et al., 2019; Niforou et al., 2014; Shonhai et al., 2011). However, consistent with their generalist nature, the challenge of maintaining large and complex proteomes has primarily been met by increased abundance of preexisting core-chaperones rather than by the *de novo* emergence of new ones. This is also reflected in their generic name 'heat-shock proteins' – under stress conditions, cells use the very same core-chaperones, yet just elevate their abundance.

In healthy cells, an integrated chaperone network, comprising both core- and co-chaperones, controls protein quality (Hipp et al., 2019; Jayaraj et al., 2020; Taipale et al., 2014). In this network (**Figure 4**), the highly abundant core-chaperones operate cooperatively, namely they do not only share, and exchange incompletely processed misfolded or unfolded protein substrates, but can also trigger the activities of one another. HSP70 plays a critical role in this network by mediating cooperative communications between the other core-chaperones. For example, HSP70 triggers the disaggregase activity of HSP100, and jointly they disaggregate aggregated proteins and promote their subsequent refolding (Glover and Lindquist, 1998; Haslberger et al., 2008; Rosenzweig et al., 2013). In another example, HSP20 can transfer misfolded substrates to HSP70 for ATP-driven unfolding, from which they can be further transferred to HSP60 for final refolding to the native state (Veinger et al., 1998). Likewise, HSP90 can promote the maturation of incompletely processed HSP70-substrates (Genest et al., 2011; Moran Luengo et al., 2018). Cooperativity and substrate-sharing between core-chaperones

are schematically represented in **Figure 4**. Together, these generalist, cooperative core-chaperones constitute the core of an integrated chaperone network that has emerged from a simple two-component system in LUCA. This core remained largely unchanged for ~3 billion years (**Figure 4**).

Alongside the expansion of proteome complexity, the chaperone network has also expanded—primarily by emergence of co-chaperones (**Figure 4**). In contrast to the generalist core-chaperones, co-chaperones are more diverse and accordingly seem to sub-specialize in specific roles, including co-chaperones that handle specific proteins. Examples include UNC45, a co-chaperone that emerged in Fungi, and facilitates HSP90-mediated maintenance of myosin in metazoan skeletal and cardiac muscles (Wohlgemuth et al., 2007). Another Fungi-born co-chaperone, Tsc1/2 heteromer, specializes in recruiting kinase and some non-kinase substrates to HSP90 (Woodford et al., 2017). Other co-chaperones mediate protein transport; examples include Tom70 and P23 that facilitate protein trafficking through Golgi and mitochondrial membranes (Craig and Marszalek, 2017; Echtenkamp et al., 2011; Melnyk et al., 2015). The specialist mode of function of co-chaperones coincides with their exponential expansion, which occurred by duplication and divergence of ancient prokaryote-born co-chaperones, but also via *bona fide* innovations, *i.e.*, by emergence of completely new specialized co-chaperones in eukaryotes. This expanding array of co-chaperones augmented the ability of core-chaperones to efficiently share substrates and to function cooperatively.

Thus, ever since the LUCA, and across the tree of life, proteome sizes have expanded exponentially, and their complexity expanded far beyond their size. New proteins with new folds have emerged continuously, also giving rise to new multi-domain proteins. Proteomes also became particularly richer in repeat and beta-rich proteins whose folding is inherently challenging. In parallel, chaperones have evolved to ensure the quality of these proteomes. Curiously, however, no new core-chaperones emerged in last ~3 billion years despite the massive, exponential expansion in proteome size and complexity that occurred during this period. Further, their gene copy numbers did not expand beyond proteome size. Instead, the challenge of exponentially expanding proteomes was met by an increase in abundance of core-chaperones, and foremost, by evolving an entire network of co-chaperones that facilitate the basal core-chaperone activity.

Author Contributions

All authors designed the research. M.R. performed the phylogenetic analysis shown in Figure 3A and 3B. M.R. and S.M. performed the chaperone copy number analysis shown in Figure 3C and 3E. S.M. performed the Tree of Life and proteome size analysis shown in Figure 1, the proteome complexity analysis shown in Figure 2, and the chaperone abundance analysis shown in Figure 3D. S.M. also prepared all the Figures. All authors discussed and commented on the results and wrote the manuscript.

Acknowledgements

We sincerely thank Jagoda Jablonska for helping to establish the representative ToL, and to Ita Gruic-Sovulj for proposing the chaperone abundance analysis. We thank Rina Rosenzweig, Harm H. Kampinga, Matthias P. Mayer, Sudip Kundu, and Agnieszka Klosowska for valuable suggestions regarding the manuscript. This work was supported by a Minerva Foundation grant to D.S.T. and Grant 31003A_175453 from the Swiss National Fund to P.G. and M.R.; S.M. was supported by PBC-VATAT Postdoctoral Fellowship, provided by the Council for Higher Education, Israel. P.G. is an Associate Professor in the Department of Plant Molecular Biology at UNIL. D.S.T. is the Nella and Leon Benoziyo Professor of Biochemistry at WIS.

Competing interests

The authors declare no competing interests.

Figure Legends

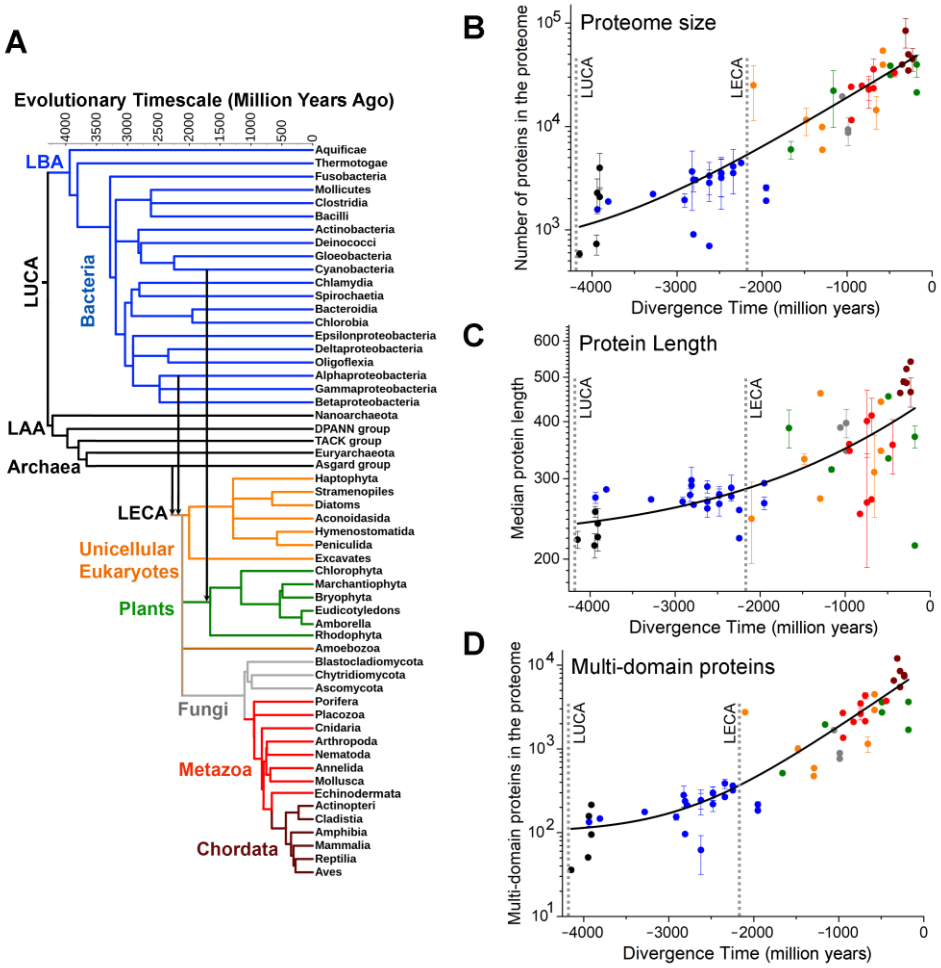

Figure 1. Expansion of proteome size in the course of evolution

(A) The Tree of Life (ToL) used in this study. Leaves represent extant phylogenetic clades, while internal nodes represent their presumed ancestors. Branch lengths correspond to the predicted evolutionary divergence time of the corresponding clades. The major phylogenetic groups in the tree (Bacteria, Archaea, Unicellular Eukaryotes, Plants, Fungi, Metazoan and Chordata) are highlighted in different colours. Vertical arrows highlight the two major endosymbiosis events: the Alphaproteobacterial origin of mitochondria and the Cyanobacterial origin of plastids. Abbreviations: LUCA: Last Universal Common Ancestor, LAA: Last Archaeal Ancestor, LBA: Last Bacterial Ancestor, LECA: Last Eukaryotic Common Ancestor.

(B–D) The average per clade values for various proteome size parameters (Y-axis, in log scale) are plotted against their predicted time of divergence (along X-axis in linear scale). These parameters include proteome size **(B)**, median protein length **(C)**, and multi-domains proteins in the proteome **(D)**. In these scatterplots, the colours of data-points represent their major phylogenetic group in the tree (panel **A**). Error bars represent the clade standard deviation (no error bars relate to clades comprising only one representative organism). The lines provide a visual representation of an exponential increase along evolutionary time as provided by the TimeTree (Hedges et al., 2015). The timelines of LUCA and LECA are highlighted with dashed vertical lines.

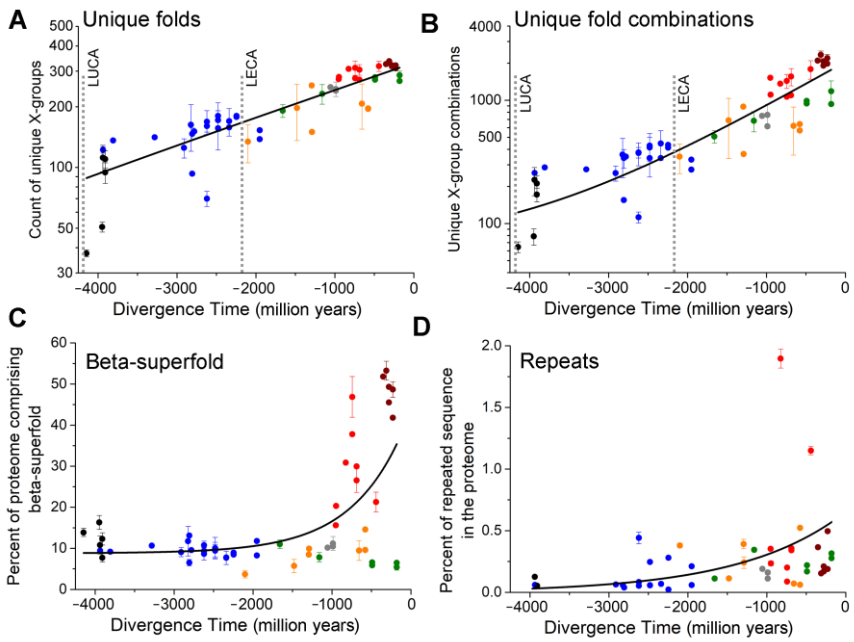

Figure 2. Exponential expansion of proteome complexity

Figure features follow those of **Figure 1**. **(A)** Shown on the Y-axis (log-scale), is the average number of unique folds (Evolutionary Classification of Domains, ECOD X-groups (Schaeffer et al., 2016)) in each phylogenetic clade.

(B) Same, for the count of unique fold combinations.

(C) Same, for the percent of proteins in the proteome comprising at least one beta-superfold domain (note the linear-scale).

(D) Same, for the percent of total proteome length that is repeat (also on linear-scale).

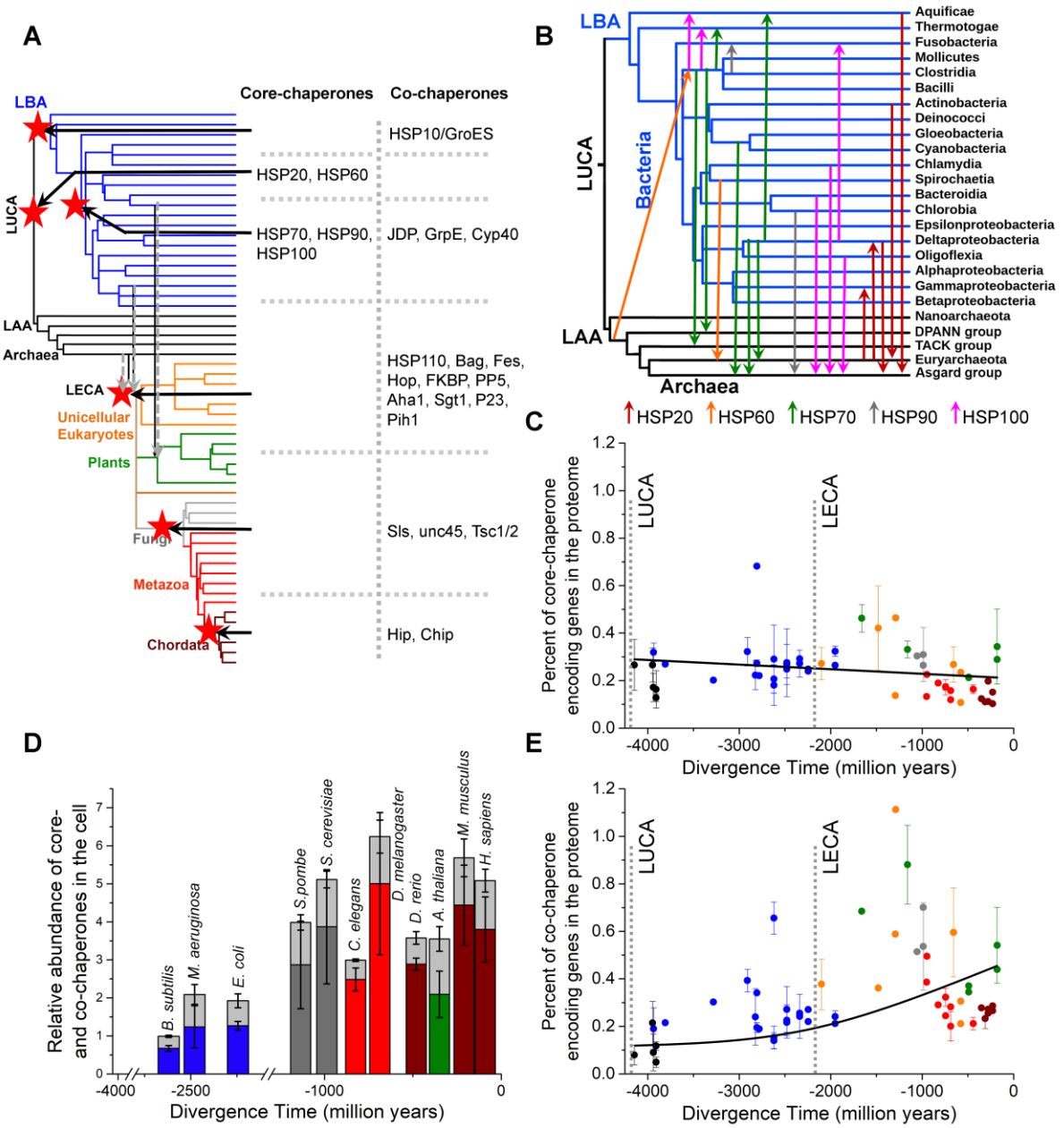

Figure 3. Evolutionary history of core- and co-chaperones

(A) The *de novo* emergence of core- and co-chaperone families are summarized on the ToL. The ToL is the same as **Figure 1A**, clade names are omitted for clarity. Ancestral nodes in which a chaperone family emerged are marked with red stars and the core- and co-chaperone families emerged in that node are listed. The dashed grey arrows reflect the endosymbiotic integration of archaeal and bacterial chaperone systems in LECA, and eukaryotic and cyanobacterial chaperone systems in photosynthetic algae.

(B) The major horizontal gene transfer (HGT) events of core-chaperones among prokaryotic clades. Shown is the prokaryotic part of the ToL with HGTs highlighted as arrows (arrow direction: donor to acceptor clade). Arrow colors refer to specific core-chaperone families, as listed in the figure. Note that position of the arrow on a branch is arbitrary and is optimized for clarity.

(C) The percent of core-chaperone genes per proteome (shown is the average percentage for each phylogenetic clade). Figure features follow **Figure 1**.

(D) The relative basal abundance of core- and co-chaperones in cells. Plotted are model organisms for which sufficient, reliable data were available against the presumed divergence time of their lineages.

The columns include core-chaperones at the bottom (colours represent the phylogenetic clade in **Figure 1A**) and co-chaperones at the top (light grey colour). The error bars represent the standard deviation among different non-redundant abundance datasets.
(E) Same as panel **C** for co-chaperone genes per proteome.

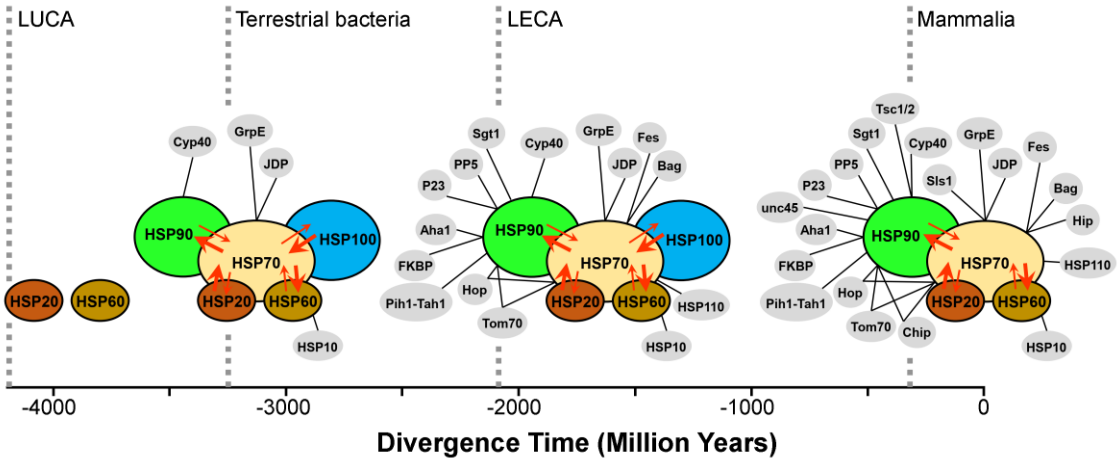

Figure 4. Evolutionary expansion of the chaperone network
A schematic representation of the integrated chaperone network at different stages of evolution. Core chaperones are shown in various colors and with black outlines, while co-chaperones are in grey with no outline. Co-chaperones of HSP60, HSP70 and HSP90 are connected to their respective core-chaperone by black lines. Cooperativity between core-chaperones is represented by overlaps between circles, and substrate sharing between different core-chaperones are shown by red arrows. Arrow direction and width represent the direction and magnitude of substrate sharing.

Supplementary Figure Legends

Figure S1 (related to Figure 1)**.** Figure features follow those of **Figure 1**. **(A)** Shown on the Y-axis (linear-scale), are the average lengths of the protein domains that belong to 38 ECOD X-groups assigned to LUCA.
(B) Same, for the length of the domain-flanking segments.
(C) Same, for the percent of proteins in the proteome comprising ≥ 3 Pfam-annotated domains.
(D) Same, for the percent of proteins in the proteome comprising < 3 Pfam-annotated domains.

Figure S2 (related to Figure 2)**.** Figure features follow those of **Figure 1**. **(A)** Shown on the Y-axis (log-scale), is the number of beta-superfold proteins in the proteome.

Figure S3 (related to Figure 2)**.** Figure features follow those of **Figure 1**. **(A)** Shown on the Y-axis (log-scale), is the total length (amino acids) of repeated sequence in the proteome.

Figure S4 (related to Figure 3)**.** Figure features follow those of **Figure 1**. Shown on the Y-axis is the average number, per genome, of genes encoding **(A)** HSP20 (note the log-scale), **(B)** HSP60, **(C)** HSP70, **(D)** HSP90, and **(E)** HSP100.

Supplementary Table Legends

Table S1 (related to Figure 3)**.** Protein trees (newick format) of core and co-chaperone families. These trees were inferred by using the Maximum Likelihood method. Initial trees for the heuristic search were obtained by NJ/BioNJ algorithm, using JTT distance model.

Supplementary Data File Legends

Data S1. The 188 representative organisms and their phylogenetic classifications (related to Figure 1).

Data S2. Numerical values of the proteome size and proteome complexity parameters (related to Figure 1 and Figure 2).

Data S3. A list of all the unique ECOD X-groups, and Pfam clans, detected in representative proteomes of our Tree of Life, and a list of ECOD X-groups assigned to LUCA (related to Figure 2).

Data S4. A list of all the unique ECOD X-group combinations detected in the representative proteomes of our Tree of Life (related to Figure 2).

Data S5. Unique Pfam domain combinations, and clan combinations, detected in the representative proteomes; 'no clan' relates to Pfam families that are not assigned to a clan, and thus reflect an independent lineage (related to Figure 2).

Data S6. Expansion of beta-superfolds beyond the expansion of proteome size: for representative organisms of our Tree of Life, shown are the percent of proteins in the proteomes that comprise a domain related to one of the ECOD top hierarchies (related to Figure 2).

Data S7. Repeat segments identified in the representative proteomes (related to Figure 2).

Data S8. Pfam-annotated domain combinations and the UniProt identifiers of the core and co-chaperones identified in the representative proteomes (related to Figure 3).

Data S9. Relative abundance of core- and co-chaperones in 11 model organisms (related to Figure 3).

Methods

Constructing the Tree of Life

To construct a representative Tree of life, we used the TimeTree database (Kumar et al., 2017) and the NCBI taxonomy database (Federhen, 2012). For all major clades of bacterial, archaeal and eukaryotic super kingdoms, non-redundant representative species were selected, ensuring that (i) the minimum splitting time for any pair of taxa is ≥ 65 million years, (ii) their annotated proteome sequences are available in NCBI genome database (Benson et al., 2013) and (iii) proteome-scale domain assignment data are available in Pfam (Finn et al., 2014). This analysis rendered 188 representative organisms covering 56 major bacterial, archaeal and eukaryotic clades (**Data S1**).

The TimeTree Database comprises phylogenetic relationships, as well as literature-based annotations of predicted emergence times (Million Years Ago, MYA, from now) for > 50,000 species. Using this database, a Tree of Life (ToL) was constructed in which leaves represent the extant clades (*e.g.*, Mammalia, which comprises three representative organisms: human, cat, and mouse). The tree's root comprises the Last Universal Common Ancestor (LUCA), and the nodes represent the hypothetical ancestors. Branch lengths represent the divergence time of the different clades. One representative species from each of our 56 phylogenetic clades was chosen, and this species set was submitted to the TimeTree Database to extract a 'core-tree' for their original tree. The obtained tree topology was manually curated and adjusted. The emergence times documented in TimeTree were originally collected from various molecular dating as well as geological studies and in our work, we used their dating as is. However, this dating should be considered as tendencies, rather than absolute numbers.

Capturing proteome complexity

Proteome size and median protein length in the proteome. Annotated proteome sequences of the 188 representative organisms were obtained as FASTA-format files from the NCBI genome database (Benson et al., 2013). For each organism, we used Biopython v1.75 package to compute the total number of proteins in the respective proteome, and the length of each protein. These protein lengths were used to estimate the median protein length for each organism (**Data S2**).

Multi-domain proteins in the proteome. Proteome-scale domain annotations of each of the 188 representative organisms were obtained from Pfam (Finn et al., 2014). In Pfam, the established profile HMMs of known domain families (Hidden Markov Models, probabilistic models used for the statistical inference of homology) are searched against the protein sequences, to find all instances of that domain. A statistical significance score (probability that the prediction is a random hit) is assigned to each predicted instance based on the sequence similarity with the profile HMM. Any domain assigned with $p < 10^{-5}$ significance were considered for further analysis. Overall, in these 188 representative

organisms, we identified 7694 domain families, which amounts to roughly 43% of all annotated domain families (17836 families) in Pfam 32.0, September 2018 release. For each species, the number of proteins comprising <3 and those comprising ≥3 Pfam-annotated domains were counted (**Data S2**).

Number of unique fold types and fold-combinations. In general, sequence homologies between different domain families show that they can be clustered into independently evolved lineages (meaning, members of different lineages do not exhibit any detectable sequence homology). Two databases, Pfam (Finn et al., 2006) and ECOD (Schaeffer et al., 2016) perform this clustering considering sequence and structural similarities among domain families as the benchmark. In Pfam, these independently evolved super-families are remarked as Clans (Finn et al., 2006). In ECOD, this clustering is hierarchical (from bottom to top: F-group, T-group, X-group, and top hierarchy) and the independently evolved lineages are termed as the X-groups (Schaeffer et al., 2016). For each of the 188 proteomes, we mapped the Pfam-assigned domains to the Pfam- Clans as well as to the ECOD X-groups. The 7694 domain families were mapped to 554 unique Clans, and to 976 X-groups, covering 88% of all annotated Clans (629 Clans in Pfam 32.0), and 42% of all annotated ECOD X-groups (2316 X-groups, ECOD v20191115). The numbers of unique Clans, or X-groups, identified in a given proteome were considered as a measure of the number of unique fold types present in a given organism (**Data S3**).

This analysis further allowed us to estimate the vectorial combinations (AB ≠ BA) of Clans / X-groups, from N- to C-terminal, present in a given protein. The total number of Clan / X-group combinations present in the proteome represents the total number of unique fold-combinations present in the respective organism. The 554 Clans and 976 X-groups included in our work yielded to 15463 X-group combinations and 16538 Clan combinations respectively (**Data S4, S5**).

Proportion of beta-superfolds in the proteome. To capture the proportion of beta-structures in the proteome, for each representative organism, we identified how many proteins in the proteome are annotated as belonging to all-beta folds, and what fraction of the entire proteome they represent. All beta structures assigned under ECOD top hierarchies beta barrel, beta meander, beta sandwich, beta duplicates or obligate multimers, and beta complex topology were considered in the analysis (**Data S6**).

Repeated sequences in the proteome. To capture the abundance of repeated sequence in the proteome, the 188 representative proteomes were scanned by T-REKS repeat-identifier program (Jorda and Kajava, 2009). All repeats that are larger than a 'foldon' unit (~20 aa) (Englander and Mayne, 2014), and exhibit ≥ 90% sequence similarity were considered for further analysis (**Data S7**). Summing the lengths of all the identified repeats, we derived the total length of repeated sequences in each proteome, and what fraction of the total proteome length it covers (total repeat length normalized by sum of all protein lengths, **Data S2**).

Expansion of domain lengths. To examine the expansion of domain lengths, we first assigned 38 ECOD X-groups to LUCA (**Data S3**), based on their presence in both *Nanoarchaeota* and *Aquificae*. Proteins harboring these X-groups were detected in the representative organisms and the respective domain lengths, as annotated in Pfam, were estimated. For each organism, these lengths were pulled together and the average domain length was estimated (**Data S2**).

Expansion of domain-flanking regions. For each protein harboring a LUCA X-group, we used the Pfam-annotated location of the protein domain in the primary sequence to estimate the lengths of C- and N-termini segments, and inter-domain linkers. For each organism, lengths of these domain-flanking regions were pulled together to estimate the average (**Data S2**).

Capturing chaperones in the proteome

To determine the evolutionary appearance and expansion of the core-chaperone (HSP20, HSP60, HSP70, HSP90, and HSP100), and co-chaperone families (HSP10/GroES, JDP/HSP40, HSP110, GrpE, Bag, Fes, Hip, Hop, Chip, Tom70, Cyp40, FKBP52/51, PP5, Unc45, Cdc37, P23, Aha1, Sgt1, Pih1, Tah1 and Tsc1/2 heterodimer) we identified their occurrences in the 188 representative organisms, using two complementary methods.

Identifying chaperones by BLAST-search. Chaperone family proteins were manually curated from the UniProt (UniProt, 2015) annotated proteomes of model organisms (*Escherichia coli* and *Saccharomyces cerevisiae*). These protein sequences were then used as queries to find orthologous sequences in the other organisms by a comprehensive protein-protein BLAST (Altschul et al., 1990). BLAST hits associated with 50% sequence coverage and $\leq 10^{-5}$ e-values (Marcet-Houben and Gabaldon, 2015) were manually inspected to extract the 'true-positive' chaperone family members.

Identifying chaperones by characteristic domain combinations. The second method involved manually looking into the Pfam-assigned domain combinations of annotated chaperones. For instance, bacterial HSP20s (*e.g.*, IbpA protein in *E. coli*) predominantly comprise a single HSP20 domain, whereas chordate HSP20s (*e.g.*, HSPB6 protein in *H. sapiens*) often comprise an additional N-terminal alpha crystallin domain. For each chaperone family, we investigated their domain organization in Pfam and constructed a library of domain combinations (occurrence of the domain of interest with other domains in annotated proteomes). This library comprised any combination that Pfam reports in at least 10 different sequences. We searched these combinations in the 188 representative proteomes. Any protein comprising any of these domain combinations was assigned to be a member of that core-chaperone family. This analysis excluded eukaryote specific HSP110 co-chaperone family that is composed of two HSP70 domains, and thus cannot be distinguished from HSP70s that comprise two HSP70 domains. In this case, specific hallmark sequences in the linker and the more variable C-terminal domain of HSP110 that differ from HSP70, were used in BLAST searches.

The two complementary methods rendered identical number of chaperone gene copy-numbers in each organism, reflecting the robustness of the overall approach (**Data S8**).

Phylogenetic analysis

Multiple sequence alignments (MSAs) were generated using Muscle v3.8.31 (Edgar, 2004). The alignments were manually curated and gap-majority columns were trimmed using trimAl v1.330 (Capella-Gutierrez et al., 2009). Only for HSP20, alignments were collected from EggNOG database (Huerta-Cepas et al., 2019), and were manually curated. These alignments were filtered by removing all sequences that are more than 80% identical (usually redundant sequences) and those that are less than 30% identical (usually interferes with rooting by creating extremely long branches) were removed using T-coffee (Di Tommaso et al., 2011). Maximum likelihood phylogenetic trees were generated by MEGA X (Kumar et al., 2018), using JTT distance matrix and NJ/BioNJ initial tree. Phylogenetics trees are provided as **Table S1**.

Chaperone abundance analysis

The abundance of a protein simply means the number of copies of a protein molecule in a cell. Non-redundant genome-scale abundance data was collected for 11 non-extremophilic model organisms from PAXdb (Wang et al., 2015), measured under normal conditions. This database comprises whole genome protein abundance information across organisms and tissues. Dataset quality was measured by its proteome coverage and interaction consistency score (ICS). Proteome coverage represents what fraction of the entire proteome is included in the abundance dataset. ICS is based on the assumption that proteins that contribute jointly to a shared function (such as members of a protein complex) should tend to have roughly similar protein abundance levels. For unicellular organisms, datasets that cover ≥40% of the respective proteomes with ≥3.0 ICS and includes ≥30% of all core- and co-chaperones identified in the respective organism, were selected for analysis. For multicellular organisms, tissue-specific data was collected. Datasets that cover ≥10% of the respective proteomes with ≥3.0 ICS and includes ≥30% of all core- and co-chaperones identified in the respective organism, were selected for analysis. All datasets related to stress or disease-conditions were removed and the remaining 121 datasets were considered for further analysis (**Data S9**). For each abundance dataset, we classified the list of proteins into three non-overlapping groups: (i) core-chaperones, (ii) co-chaperones and (iii) proteins that are not chaperones. For each group, the abundance values of all the proteins were summed to estimate the 'total abundance'. The 'total abundance of core-chaperones', normalized by the 'total abundance of proteins that are not chaperones' represents the relative abundance of core-chaperones. Similarly we estimated the 'relative abundance of co-chaperones'. For each species, the average and standard deviations among different datasets were measured.

Visualizing the expansion of proteome complexity and of chaperones

For each clade in our core-tree, the proteome complexity and chaperone-copy number values obtained for its representative organisms were pulled together to estimate the clade average, and the clade standard deviation. The clade average values were subsequently plotted against their predicted divergence time and were fitted into the standard exponential growth curve. The fitted exponential curves are depicted as solid black lines.

Graphics

The Tree of Life was generated using the Interactive Tree Of Life (iTOL) v4.0 (Letunic and Bork, 2019). All the plots were generated using OriginPro software v9.1.0. Figures were compiled using Adobe Photoshop CS6 v13.0.1.

Quantification and statistical analysis

All the statistical analyses mentioned in the main text were performed using in-house Python and R scripts.

Bibliography

Altschul, S.F., Gish, W., Miller, W., Myers, E.W., and Lipman, D.J. (1990). Basic local alignment search tool. J Mol Biol *215*, 403-410.

Alvarez-Ponce, D., Aguilar-Rodriguez, J., and Fares, M.A. (2019). Molecular Chaperones Accelerate the Evolution of Their Protein Clients in Yeast. Genome Biol Evol *11*, 2360-2375.

Andrade, M.A., Perez-Iratxeta, C., and Ponting, C.P. (2001). Protein repeats: structures, functions, and evolution. J Struct Biol *134*, 117-131.

Anfinsen, C.B. (1973). Principles that govern the folding of protein chains. Science *181*, 223-230.

Arendt, D. (2008). The evolution of cell types in animals: emerging principles from molecular studies. Nat Rev Genet *9*, 868-882.

Battistuzzi, F.U., Feijao, A., and Hedges, S.B. (2004). A genomic timescale of prokaryote evolution: insights into the origin of methanogenesis, phototrophy, and the colonization of land. BMC Evol Biol *4*, 44.

Battistuzzi, F.U., and Hedges, S.B. (2009). A major clade of prokaryotes with ancient adaptations to life on land. Mol Biol Evol *26*, 335-343.

Benson, D.A., Cavanaugh, M., Clark, K., Karsch-Mizrachi, I., Lipman, D.J., Ostell, J., and Sayers, E.W. (2013). GenBank. Nucleic Acids Res *41*, D36-42.

Bogumil, D., Alvarez-Ponce, D., Landan, G., McInerney, J.O., and Dagan, T. (2014). Integration of two ancestral chaperone systems into one: the evolution of eukaryotic molecular chaperones in light of eukaryogenesis. Mol Biol Evol *31*, 410-418.

Bogumil, D., and Dagan, T. (2012). Cumulative impact of chaperone-mediated folding on genome evolution. Biochemistry *51*, 9941-9953.

Bukau, B., and Horwich, A.L. (1998). The Hsp70 and Hsp60 Chaperone Machines. Cell *92*, 351-366.

Capella-Gutierrez, S., Silla-Martinez, J.M., and Gabaldon, T. (2009). trimAl: a tool for automated alignment trimming in large-scale phylogenetic analyses. Bioinformatics *25*, 1972-1973.

Caplan, A.J. (2003). What is a co-chaperone? Cell Stress Chaperones *8*, 105-107.

Cooper, G., and Hausman, R.E. (2000). The cell ; a molecular approach (Oxford: Sinauer Associates).

Craig, E.A., and Marszalek, J. (2017). How Do J-Proteins Get Hsp70 to Do So Many Different Things? Trends Biochem Sci *42*, 355-368.

Dahl, J.U., Gray, M.J., and Jakob, U. (2015). Protein quality control under oxidative stress conditions. J Mol Biol *427*, 1549-1563.

Day, J., Passecker, A., Beck, H.P., and Vakonakis, I. (2019). The Plasmodium falciparum Hsp70-x chaperone assists the heat stress response of the malaria parasite. Faseb j *33*, 14611-14624.

de Duve, C. (2007). The origin of eukaryotes: a reappraisal. Nat Rev Genet *8*, 395-403.

Di Giulio, M. (2007). The tree of life might be rooted in the branch leading to Nanoarchaeota. Gene *401*, 108-113.

Di Tommaso, P., Moretti, S., Xenarios, I., Orobitg, M., Montanyola, A., Chang, J.M., Taly, J.F., and Notredame, C. (2011). T-Coffee: a web server for the multiple sequence alignment of protein and RNA sequences using structural information and homology extension. Nucleic Acids Res *39*, W13-17.

Dill, K.A., and Chan, H.S. (1997). From Levinthal to pathways to funnels. Nat Struct Biol *4*, 10-19.

Doolittle, W.F. (1999). Phylogenetic classification and the universal tree. Science *284*, 2124-2129.

Duncan, E.J., Cheetham, M.E., Chapple, J.P., and van der Spuy, J. (2015). The role of HSP70 and its co-chaperones in protein misfolding, aggregation and disease. Subcell Biochem *78*, 243-273.

Echtenkamp, F.J., Zelin, E., Oxelmark, E., Woo, J.I., Andrews, B.J., Garabedian, M., and Freeman, B.C. (2011). Global functional map of the p23 molecular chaperone reveals an extensive cellular network. Mol Cell *43*, 229-241.

Edgar, R.C. (2004). MUSCLE: multiple sequence alignment with high accuracy and high throughput. Nucleic Acids Res *32*, 1792-1797.

Eme, L., Spang, A., Lombard, J., Stairs, C.W., and Ettema, T.J.G. (2017). Archaea and the origin of eukaryotes. Nat Rev Microbiol *15*, 711-723.

Englander, S.W., and Mayne, L. (2014). The nature of protein folding pathways. Proc Natl Acad Sci U S A *111*, 15873-15880.

Federhen, S. (2012). The NCBI Taxonomy database. Nucleic Acids Res *40*, D136-143.

Fernandez-Fernandez, M.R., and Valpuesta, J.M. (2018). Hsp70 chaperone: a master player in protein homeostasis. F1000Res *7*.

Finka, A., Mattoo, R.U., and Goloubinoff, P. (2016). Experimental Milestones in the Discovery of Molecular Chaperones as Polypeptide Unfolding Enzymes. Annu Rev Biochem *85*, 715-742.

Finn, R.D., Bateman, A., Clements, J., Coggill, P., Eberhardt, R.Y., Eddy, S.R., Heger, A., Hetherington, K., Holm, L., Mistry, J., *et al.* (2014). Pfam: the protein families database. Nucleic Acids Res *42*, D222-230.

Finn, R.D., Mistry, J., Schuster-Bockler, B., Griffiths-Jones, S., Hollich, V., Lassmann, T., Moxon, S., Marshall, M., Khanna, A., Durbin, R., *et al.* (2006). Pfam: clans, web tools and services. Nucleic Acids Res *34*, D247-251.

Fournier, G.P., and Poole, A.M. (2018). A Briefly Argued Case That Asgard Archaea Are Part of the Eukaryote Tree. Front Microbiol *9*, 1896.

Genest, O., Hoskins, J.R., Camberg, J.L., Doyle, S.M., and Wickner, S. (2011). Heat shock protein 90 from Escherichia coli collaborates with the DnaK chaperone system in client protein remodeling. Proc Natl Acad Sci U S A *108*, 8206-8211.

Glover, J.R., and Lindquist, S. (1998). Hsp104, Hsp70, and Hsp40: a novel chaperone system that rescues previously aggregated proteins. Cell *94*, 73-82.

Gong, Y., Kakihara, Y., Krogan, N., Greenblatt, J., Emili, A., Zhang, Z., and Houry, W.A. (2009). An atlas of chaperone-protein interactions in Saccharomyces cerevisiae: implications to protein folding pathways in the cell. Mol Syst Biol *5*, 275.

Halaby, D.M., and Mornon, J.P. (1998). The immunoglobulin superfamily: an insight on its tissular, species, and functional diversity. J Mol Evol *46*, 389-400.

Han, J.H., Batey, S., Nickson, A.A., Teichmann, S.A., and Clarke, J. (2007). The folding and evolution of multidomain proteins. Nat Rev Mol Cell Biol *8*, 319-330.

Haslberger, T., Zdanowicz, A., Brand, I., Kirstein, J., Turgay, K., Mogk, A., and Bukau, B. (2008). Protein disaggregation by the AAA+ chaperone ClpB involves partial threading of looped polypeptide segments. Nat Struct Mol Biol *15*, 641-650.

Hedges, S.B., Marin, J., Suleski, M., Paymer, M., and Kumar, S. (2015). Tree of life reveals clock-like speciation and diversification. Mol Biol Evol *32*, 835-845.

Heim, N.A., Payne, J.L., Finnegan, S., Knope, M.L., Kowalewski, M., Lyons, S.K., McShea, D.W., Novack-Gottshall, P.M., Smith, F.A., and Wang, S.C. (2017). Hierarchical complexity and the size limits of life. Proc Biol Sci *284*, 20171039.

Hemmingsen, S.M., Woolford, C., van der Vies, S.M., Tilly, K., Dennis, D.T., Georgopoulos, C.P., Hendrix, R.W., and Ellis, R.J. (1988). Homologous plant and bacterial proteins chaperone oligomeric protein assembly. Nature *333*, 330-334.

Henzler-Wildman, K., and Kern, D. (2007). Dynamic personalities of proteins. Nature *450*, 964-972.

Hipp, M.S., Kasturi, P., and Hartl, F.U. (2019). The proteostasis network and its decline in ageing. Nat Rev Mol Cell Biol *20*, 421-435.

Huerta-Cepas, J., Szklarczyk, D., Heller, D., Hernandez-Plaza, A., Forslund, S.K., Cook, H., Mende, D.R., Letunic, I., Rattei, T., Jensen, L.J., *et al.* (2019). eggNOG 5.0: a hierarchical, functionally and phylogenetically annotated orthology resource based on 5090 organisms and 2502 viruses. Nucleic Acids Res *47*, D309-D314.

Jayaraj, G.G., Hipp, M.S., and Hartl, F.U. (2020). Functional Modules of the Proteostasis Network. Cold Spring Harb Perspect Biol *12*.

Jorda, J., and Kajava, A.V. (2009). T-REKS: identification of Tandem REpeats in sequences with a K-meanS based algorithm. Bioinformatics *25*, 2632-2638.

Kampinga, H.H., Andreasson, C., Barducci, A., Cheetham, M.E., Cyr, D., Emanuelsson, C., Genevaux, P., Gestwicki, J.E., Goloubinoff, P., Huerta-Cepas, J., *et al.* (2019). Function, evolution, and structure of J-domain proteins. Cell Stress Chaperones *24*, 7-15.

Kampinga, H.H., Hageman, J., Vos, M.J., Kubota, H., Tanguay, R.M., Bruford, E.A., Cheetham, M.E., Chen, B., and Hightower, L.E. (2009). Guidelines for the nomenclature of the human heat shock proteins. Cell Stress Chaperones *14*, 105-111.

Kim, Y.E., Hipp, M.S., Bracher, A., Hayer-Hartl, M., and Hartl, F.U. (2013). Molecular chaperone functions in protein folding and proteostasis. Annu Rev Biochem *82*, 323-355.

Kriehuber, T., Rattei, T., Weinmaier, T., Bepperling, A., Haslbeck, M., and Buchner, J. (2010). Independent evolution of the core domain and its flanking sequences in small heat shock proteins. FASEB J *24*, 3633-3642.

Kumar, S., Stecher, G., Li, M., Knyaz, C., and Tamura, K. (2018). MEGA X: Molecular Evolutionary Genetics Analysis across Computing Platforms. Mol Biol Evol *35*, 1547-1549.

Kumar, S., Stecher, G., Suleski, M., and Hedges, S.B. (2017). TimeTree: A Resource for Timelines, Timetrees, and Divergence Times. Mol Biol Evol *34*, 1812-1819.

Lafita, A., Tian, P., Best, R.B., and Bateman, A. (2019). Tandem domain swapping: determinants of multidomain protein misfolding. Curr Opin Struct Biol *58*, 97-104.

Letunic, I., and Bork, P. (2019). Interactive Tree Of Life (iTOL) v4: recent updates and new developments. Nucleic Acids Res *47*, W256-W259.

Liu, K., Maciuba, K., and Kaiser, C.M. (2019). The Ribosome Cooperates with a Chaperone to Guide Multi-domain Protein Folding. Mol Cell *74*, 310-319 e317.

MacLeod, F., Kindler, G.S., Wong, H.L., Chen, R., and Burns, B.P. (2019). Asgard archaea: Diversity, function, and evolutionary implications in a range of microbiomes. AIMS Microbiol *5*, 48-61.

Marcet-Houben, M., and Gabaldon, T. (2015). Beyond the Whole-Genome Duplication: Phylogenetic Evidence for an Ancient Interspecies Hybridization in the Baker's Yeast Lineage. PLoS Biol *13*, e1002220.

Margulis, L., Chapman, M., Guerrero, R., and Hall, J. (2006). The last eukaryotic common ancestor (LECA): Acquisition of cytoskeletal motility from aerotolerant spirochetes in the Proterozoic Eon. Proc Natl Acad Sci U S A *103*, 13080-13085.

Martin, W., Rujan, T., Richly, E., Hansen, A., Cornelsen, S., Lins, T., Leister, D., Stoebe, B., Hasegawa, M., and Penny, D. (2002). Evolutionary analysis of Arabidopsis, cyanobacterial, and chloroplast genomes reveals plastid phylogeny and thousands of cyanobacterial genes in the nucleus. Proc Natl Acad Sci U S A *99*, 12246-12251.

Martin, W., Stoebe, B., Goremykin, V., Hapsmann, S., Hasegawa, M., and Kowallik, K.V. (1998). Gene transfer to the nucleus and the evolution of chloroplasts. Nature *393*, 162-165.

Mayer, M.P. (2010). Gymnastics of molecular chaperones. Mol Cell *39*, 321-331.

Melnyk, A., Rieger, H., and Zimmermann, R. (2015). Co-chaperones of the mammalian endoplasmic reticulum. Subcell Biochem *78*, 179-200.

Moran Luengo, T., Kityk, R., Mayer, M.P., and Rudiger, S.G.D. (2018). Hsp90 Breaks the Deadlock of the Hsp70 Chaperone System. Mol Cell *70*, 545-552 e549.

Niforou, K., Cheimonidou, C., and Trougakos, I.P. (2014). Molecular chaperones and proteostasis regulation during redox imbalance. Redox Biol *2*, 323-332.

Pawar, A.P., DuBay, K.F., Zurdo, J., Chiti, F., Vendruscolo, M., and Dobson, C.M. (2005). Prediction of “Aggregation-prone” and “Aggregation-susceptible” Regions in Proteins Associated with Neurodegenerative Diseases. J Mol Biol *350*, 379-392.

Rosenzweig, R., Moradi, S., Zarrine-Afsar, A., Glover, J.R., and Kay, L.E. (2013). Unraveling the mechanism of protein disaggregation through a ClpB-DnaK interaction. Science *339*, 1080-1083.

Rosenzweig, R., Nillegoda, N.B., Mayer, M.P., and Bukau, B. (2019). The Hsp70 chaperone network. Nat Rev Mol Cell Biol.

Rudiger, S., Germeroth, L., Schneider-Mergener, J., and Bukau, B. (1997). Substrate specificity of the DnaK chaperone determined by screening cellulose-bound peptide libraries. EMBO J *16*, 1501-1507.

Saibil, H. (2013). Chaperone machines for protein folding, unfolding and disaggregation. Nat Rev Mol Cell Biol *14*, 630-642.

Sarkar, N.K., Kundnani, P., and Grover, A. (2013). Functional analysis of Hsp70 superfamily proteins of rice (Oryza sativa). Cell Stress Chaperones *18*, 427-437.

Schaeffer, R.D., Liao, Y., Cheng, H., and Grishin, N.V. (2016). ECOD: new developments in the evolutionary classification of domains. Nucleic Acids Research *45*, D296-D302.

Scheibel, T., Weikl, T., and Buchner, J. (1998). Two chaperone sites in Hsp90 differing in substrate specificity and ATP dependence. Proc Natl Acad Sci U S A *95*, 1495-1499.

Schopf, F.H., Biebl, M.M., and Buchner, J. (2017). The HSP90 chaperone machinery. Nat Rev Mol Cell Biol *18*, 345-360.

Shonhai, A., Maier, A.G., Przyborski, J.M., and Blatch, G.L. (2011). Intracellular protozoan parasites of humans: the role of molecular chaperones in development and pathogenesis. Protein Pept Lett *18*, 143-157.

Sousa, F.L., Nelson-Sathi, S., and Martin, W.F. (2016). One step beyond a ribosome: The ancient anaerobic core. Biochim Biophys Acta *1857*, 1027-1038.

Spang, A., Eme, L., Saw, J.H., Caceres, E.F., Zaremba-Niedzwiedzka, K., Lombard, J., Guy, L., and Ettema, T.J.G. (2018). Asgard archaea are the closest prokaryotic relatives of eukaryotes. PLoS Genet *14*, e1007080.

Taipale, M., Tucker, G., Peng, J., Krykbaeva, I., Lin, Z.-Y., Larsen, B., Choi, H., Berger, B., Gingras, A.-C., and Lindquist, S. (2014). A Quantitative Chaperone Interaction Network Reveals the Architecture of Cellular Protein Homeostasis Pathways. Cell *158*, 434-448.

Tawfik, D.S., and Gruic-Sovulj, I. (2020). How evolution shapes enzyme selectivity - lessons from aminoacyl-tRNA synthetases and other amino acid utilizing enzymes. FEBS J *287*, 1284-1305.

Techtmann, S.M., and Robb, F.T. (2010). Archaeal-like chaperonins in bacteria. Proc Natl Acad Sci U S A *107*, 20269-20274.

Tokuriki, N., and Tawfik, D.S. (2009). Protein Dynamism and Evolvability. Science *324*, 203-207.

UniProt, C. (2015). UniProt: a hub for protein information. Nucleic Acids Res *43*, D204-212.

Van de Peer, Y., Maere, S., and Meyer, A. (2009). The evolutionary significance of ancient genome duplications. Nat Rev Genet *10*, 725-732.

Veinger, L., Diamant, S., Buchner, J., and Goloubinoff, P. (1998). The small heat-shock protein IbpB from Escherichia coli stabilizes stress-denatured proteins for subsequent refolding by a multichaperone network. J Biol Chem *273*, 11032-11037.

Wang, M., Herrmann, C.J., Simonovic, M., Szklarczyk, D., and von Mering, C. (2015). Version 4.0 of PaxDb: Protein abundance data, integrated across model organisms, tissues, and cell-lines. Proteomics *15*, 3163-3168.

Waters, E., Hohn, M.J., Ahel, I., Graham, D.E., Adams, M.D., Barnstead, M., Beeson, K.Y., Bibbs, L., Bolanos, R., Keller, M., *et al.* (2003). The genome of Nanoarchaeum equitans: insights into early archaeal evolution and derived parasitism. Proc Natl Acad Sci U S A *100*, 12984-12988.

Weiss, M.C., Sousa, F.L., Mrnjavac, N., Neukirchen, S., Roettger, M., Nelson-Sathi, S., and Martin, W.F. (2016). The physiology and habitat of the last universal common ancestor. Nat Microbiol *1*, 16116.

Woese, C. (1998). The universal ancestor. Proceedings of the National Academy of Sciences *95*, 6854-6859.

Wohlgemuth, S.L., Crawford, B.D., and Pilgrim, D.B. (2007). The myosin co-chaperone UNC-45 is required for skeletal and cardiac muscle function in zebrafish. Dev Biol *303*, 483-492.

Woodford, M.R., Sager, R.A., Marris, E., Dunn, D.M., Blanden, A.R., Murphy, R.L., Rensing, N., Shapiro, O., Panaretou, B., Prodromou, C., *et al.* (2017). Tumor suppressor Tsc1 is a new Hsp90 co-chaperone that facilitates folding of kinase and non-kinase clients. Embo J *36*, 3650-3665.

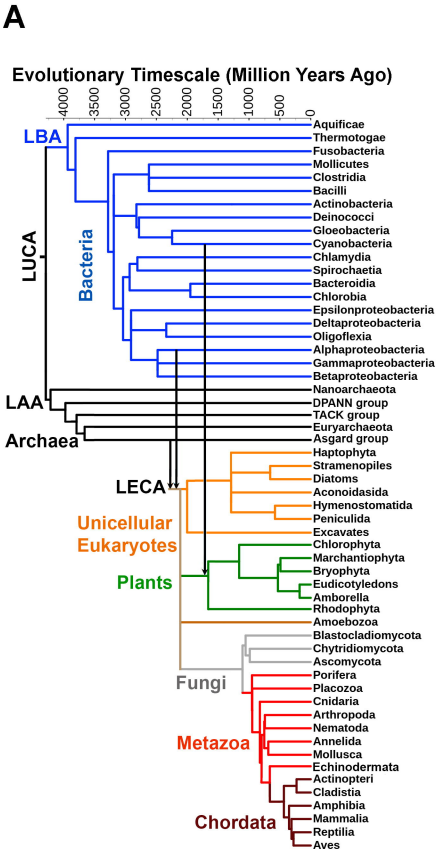
A
Evolutionary Timescale (Million Years Ago)
-4000
-3500
-3000
-2500
-2000
-1500
-1000
-500
0
LBA
LUCA
Bacteria
LAA
Archaea
LECA
Unicellular Eukaryotes
Plants
Fungi
Metazoa
Chordata
Aquificae
Thermotogae
Fusobacteria
Mollicutes
Clostridia
Bacilli
Actinobacteria
Deinococci
Gloeobacteria
Cyanobacteria
Chlamydia
Spirochaetia
Bacteroidia
Chlorobia
Epsilonproteobacteria
Deltaproteobacteria
Oligoflexia
Alphaproteobacteria
Gammaproteobacteria
Betaproteobacteria
Nanoarchaeota
DPANN group
TACK group
Euryarchaeota
Asgard group
Haptophyta
Stramenopiles
Diatoms
Aconoidasida
Hymenostomatida
Peniculida
Excavates
Chlorophyta
Marchantiophyta
Bryophyta
Eudicotyledons
Amborella
Rhodophyta
Amoebozoa
Blastocladiomycota
Chytridiomycota
Ascomycota
Porifera
Placozoa
Cnidaria
Arthropoda
Nematoda
Annelida
Mollusca
Echinodermata
Actinopteri
Cladistia
Amphibia
Mammalia
Reptilia
Aves

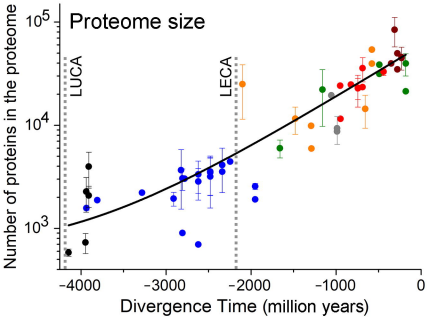
B
Proteome size
Number of proteins in the proteome
10^5
10^4
10^3
LUCA
LECA
-4000
-3000
-2000
-1000
0
Divergence Time (million years)

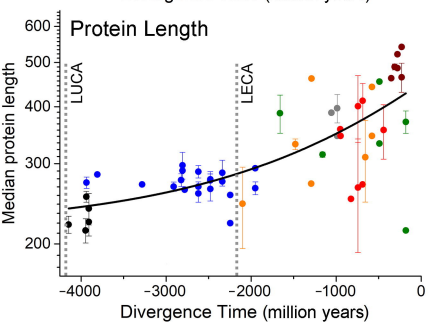
C
Protein Length
Median protein length
600
500
400
300
200
LUCA
LECA
-4000
-3000
-2000
-1000
0
Divergence Time (million years)

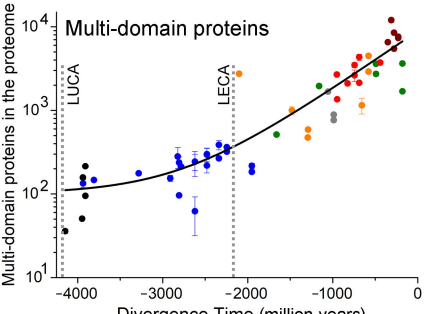
D
Multi-domain proteins
Multi-domain proteins in the proteome
10^4
10^3
10^2
10^1
LUCA
LECA
-4000
-3000
-2000
-1000
0
Divergence Time (million years)

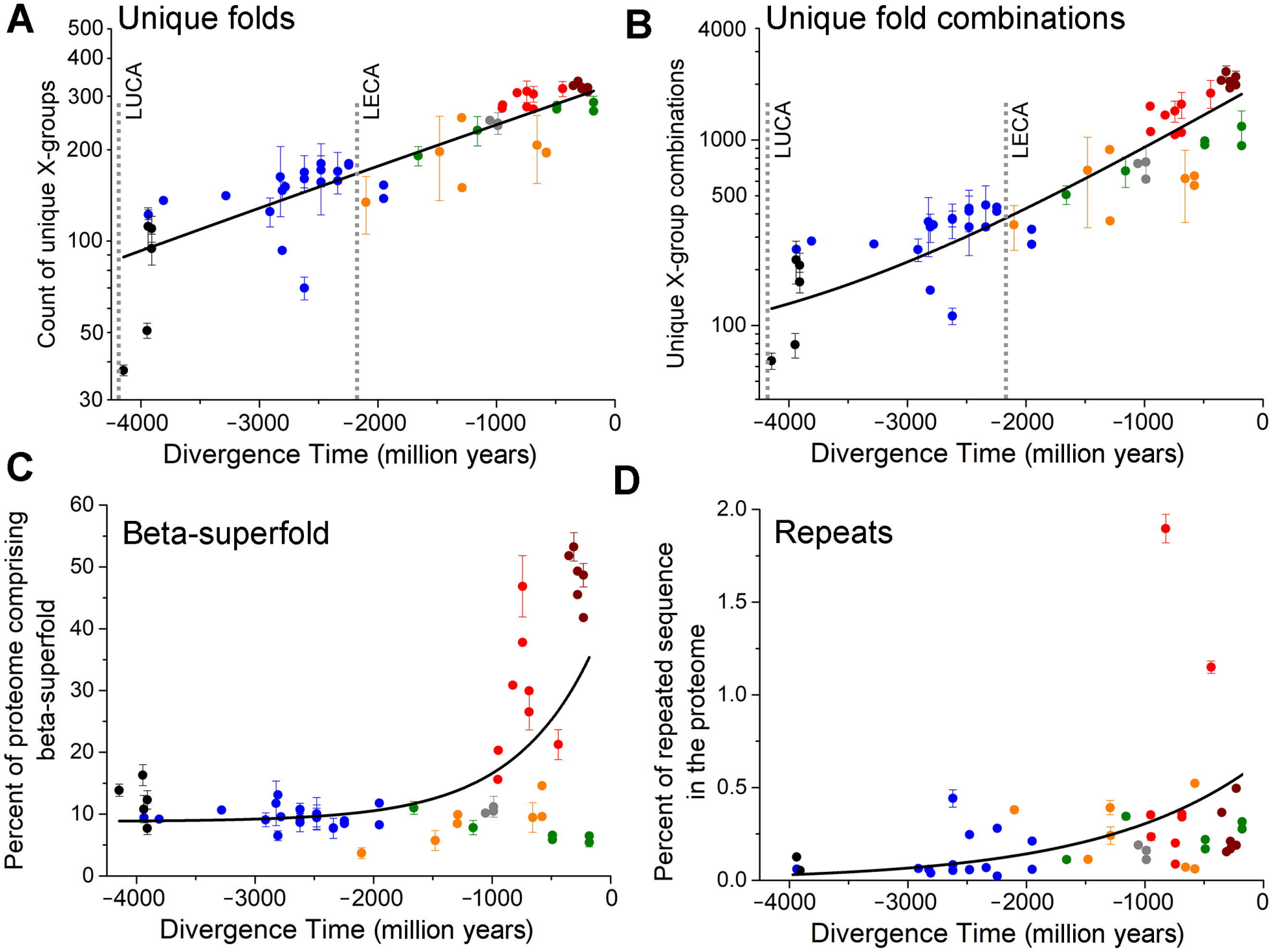
A
Unique folds
Count of unique X-groups
LUCA
LECA
Divergence Time (million years)
B
Unique fold combinations
Unique X-group combinations
LUCA
LECA
Divergence Time (million years)
C
Beta-superfold
Percent of proteome comprising beta-superfold
Divergence Time (million years)
D
Repeats
Percent of repeated sequence in the proteome
Divergence Time (million years)

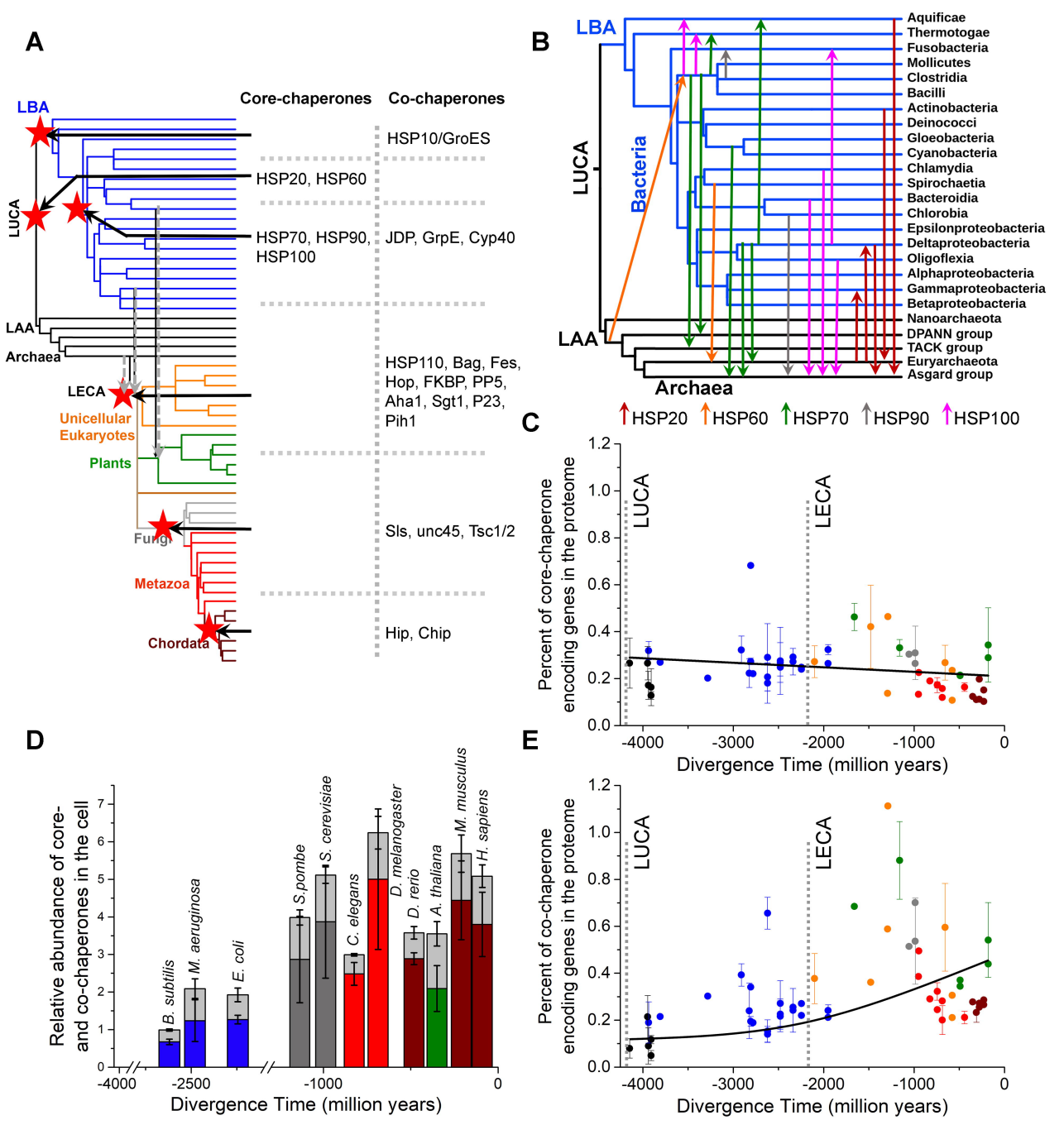
A
Core-chaperones
Co-chaperones
LBA
LUCA
LAA
Archaea
LECA
Unicellular Eukaryotes
Plants
Fungi
Metazoa
Chordata
HSP10/GroES
HSP20, HSP60
HSP70, HSP90, HSP100
JDP, GrpE, Cyp40
HSP110, Bag, Fes, Hop, FKBP, PP5, Aha1, Sgt1, P23, Pih1
Sls, unc45, Tsc1/2
Hip, Chip
B
LBA
LUCA
Bacteria
LAA
Archaea
Aquificae
Thermotogae
Fusobacteria
Mollicutes
Clostridia
Bacilli
Actinobacteria
Deinococci
Gloeobacteria
Cyanobacteria
Chlamydia
Spirochaetia
Bacteroidia
Chlorobia
Epsilonproteobacteria
Deltaproteobacteria
Oligoflexia
Alphaproteobacteria
Gammaproteobacteria
Betaproteobacteria
Nanoarchaeota
DPANN group
TACK group
Euryarchaeota
Asgard group
HSP20
HSP60
HSP70
HSP90
HSP100
C
Percent of core-chaperone encoding genes in the proteome
LUCA
LECA
Divergence Time (million years)
D
Relative abundance of core- and co-chaperones in the cell
B. subtilis
M. aeruginosa
E. coli
S.pombe
S. cerevisiae
C. elegans
D. melanogaster
D. rerio
A. thaliana
M. musculus
H. sapiens
Divergence Time (million years)
E
Percent of co-chaperone encoding genes in the proteome
LUCA
LECA
Divergence Time (million years)

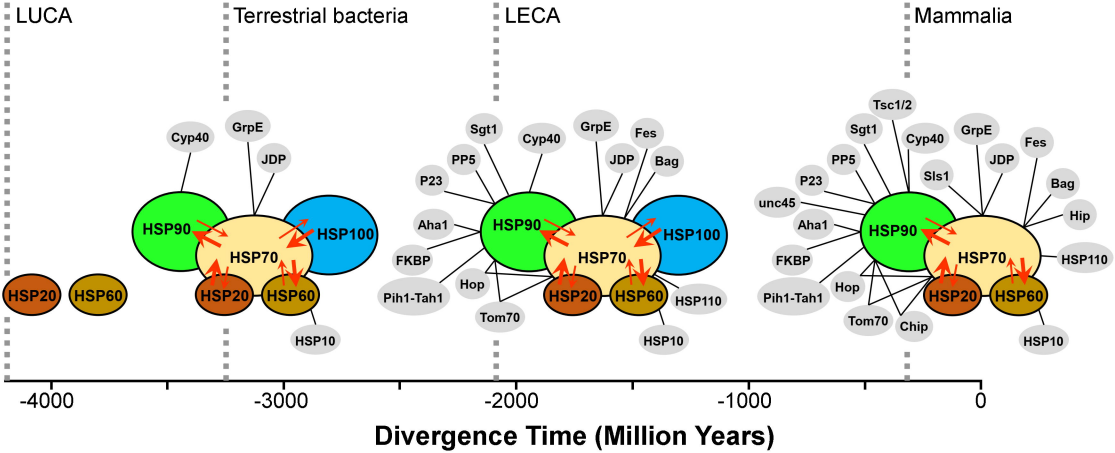
LUCA
Terrestrial bacteria
LECA
Mammalia
HSP20
HSP60
Cyp40
GrpE
JDP
HSP90
HSP70
HSP100
HSP20
HSP60
HSP10
Sgt1
PP5
P23
Aha1
FKBP
Pih1-Tah1
Hop
Tom70
Cyp40
GrpE
Fes
JDP
Bag
HSP90
HSP70
HSP100
HSP20
HSP60
HSP110
HSP10
Tsc1/2
Sgt1
Cyp40
GrpE
Fes
PP5
Sls1
JDP
Bag
P23
unc45
Hip
Aha1
HSP90
HSP70
HSP110
FKBP
Hop
Pih1-Tah1
HSP20
HSP60
Tom70
Chip
HSP10
-4000
-3000
-2000
-1000
0
Divergence Time (Million Years)